ELSEVIER

Journal of Molecular Catalysis A: Chemical 192 (2003) 9–24

JOURNAL OF MOLECULAR CATALYSIS A: CHEMICAL

www.elsevier.com/locate/molcata

DFT studies of zirconocene/MAO interaction

P.G. Belelli, M.M. Branda, N.J. Castellani*

Departamento de Física (UNS) Avenida Alem 1252, 8000 Bahía Blanca, Argentina

Received 25 March 2002; received in revised form 15 April 2002; accepted 8 July 2002

Abstract

A theoretical study of Cp_2ZrCl_2/MAO system is presented based on Density Functional Theory (DFT) calculations performed with gaussian basis-sets. The MAO cocatalyst was modeled as a small finite section of the most probably species in solution. The geometry of the cation–counterion forming the ionic-pair active site was fully optimized and its electronic structure was examined in terms of the Natural Bond Orbital (NBO) population analysis. In this way the ionic-pair interaction can be related to the electronic charge changes around the zirconium cation. The results indicate the formation of a stable ionic-pair and the redistribution of charge in the cation complex and counterion. The latter was concluded by mapping the charge density difference. The Laplacian of charge density confirm the ionic interaction of the metallocene/MAO system.

Keywords: MO calculations; DFT; Metallocene catalysts; MAO cocatalyst

1. Introduction

In last years, a great deal of transition metal complexes usually employed as catalytic precursors and organometallic compounds acting as cocatalyts have been considered for polymerization of α-olefins. Those complexes of group IVB (Ti, Zr and Hf) have been the most promising because these metallocenic catalytic systems allow a high degree of control on the polymer microstructure. For this reason, they may be considered as the next generation of catalysts for polymerization of α-olefins.

At present, metallocene catalysts are objects of increasing research particularly focusing on its stereochemical properties. The stereoselectivity in polymerization of propylene and higher α-olefins is, to a large proportion, due to the ligands forming the complex. The steric hindrance of active center and the electronic modification due to π ligands are two very important factors that determine metallocene performance, particularly affecting the catalytic activity and the quality of the produced polymer [1,2]. However, metallocene complexes are not catalytically active by themselves. They need a cocatalytic action to polymerize. In the past, a great deal of cocatalysts has been studied. Up to date, methylaluminoxane (MAO) continues being the best cocatalyst. This complex compound is usually expressed as $[–Al(CH_3)O–]_n$ (with $n = 6$–20), formed during the controlled hydrolysis of trimethyaluminium [3].

In whole literature, most of theoretical papers have been concerned with searching which are the more likely metallocene mechanisms required to produce stereoregular polymers. Different theoretical methods have been used as tools to study the reactive properties

* Corresponding author. Tel.: +54-291-4595141; fax: +54-291-4595142.
E-mail addresses: pbelelli@criba.edu.ar (P.G. Belelli), castella@criba.edu.ar (N.J. Castellani).

1381-1169/02/$ – see front matter
PII: S1381-1169(02)00404-1

of such active sites: first principles, both ab initio and Density Functional Theory (DFT), semiempirical and molecular mechanic methods. Angermund et al. [4] evaluated different models to select the best for describing the zirconocene geometry by means of energy minimization. In general the Zr-ligand π-bond was analyzed taking into account three different models: "funnel", "ionic" and "centroid". The centroid model was the more convenient to describe the metallocene geometry and to represent NMR experiments (free rotation of the ligand trough the metal–ligand π-bond).

In almost every theoretical work reported in literature about the nature of these active sites the zircocation was considered as an isolated species [5]. The justification for this hypothesis is that the presence of a free ion is a sufficient (but not necessary) condition to be fulfilled to produce the olefin polymerization. Nevertheless, one of the most important questions of the cationic model is the energy required to dissociate the ion-pair. This energy can hardly be compensated for by the solvatation energy in the weakly polar solvent usually used in olefin polymerization. Fusco et al. [6] evaluated the energy to separate $Cp_2TiCH_3^+$ from $Al(CH_3)_2Cl_2^-$ in vacuum. They found a value bigger than 100 kcal/mol. Besides, an isolated cation which is a species extremely electron-deficient and highly coordinately unsaturated is very exposed to undergo decomposition. In this regard, a certain degree of coordination coming from anion or solvent is required to avoid the irreversible decomposition processes.

From previous results obtained by Fusco et al. [7], a subsequent paper was performed assuming the presence of the cocatalyst near the active center. By means of DFT, these authors investigated the energy differences among three proposed intermediate species. They point out that even when the DFT study shows that a negative charge dispersion in MAO macroanions strongly reduces the ion-pair dissociation energy, this result cannot justify by itself the formation of free cationic species [8].

In the past, the main goal of theoretical approaches has been to study the polymerization mechanisms, particularly those reactions related to the olefin coordination (ethylene and propylene monomers) and to the monomer insertion into the metal–C bond. As it was above mentioned the most used model for the active site was the isolated cation with different alkyl ligands, without counterion. Nevertheless, some authors underlined that the role of cocatalyts, counter ion, or solvents in this catalytic process is very important to describe realistic active sites [9].

The aim of the present work is to give a more complete description of a polymerization reactive site based on the simplest non-bridged *bis*-chlorozirconocene (Cp_2ZrCl_2) as cationic species ($Cp_2ZrCH_3^+$) and MAO as counterion. The electronic structure of each of these species and the interaction between them were analyzed with different theoretical tools. For the construction of MAO model we took into account the theoretical considerations and experimental results collected in the last few years.

As it was mentioned above, the presence of cocatalyst is of major importance because the metallocene molecule by itself is not active. In this work the interaction between zirconocene and cocatalyst has been examined in order to define the most stable species.

The role of cocatalyst, in our case MAO, is widely known to be significant in several aspects: (i) alkylation of a catalyst precursor like the metallocene dichloride (Cp_2ZrCl_2), (ii) generation of a cationic zirconocene complex, (iii) stabilization of cationic complexes acting as counterion, and (iv) reactivation of deactivated sites [10,11]. In this work only the steps (ii) and (iii) are examined.

When the zirconocene Cp_2ZrCl_2 complex reacts with a MAO molecule the monomethylated $Cp_2ZrClCH_3$ precursor and MAOCl are produced (Eq. (1)). This reaction is usually designed as the first alkylation, due to the exchange of a Cl atom of zirconocene and a methyl group of cocatalyst. In a second step, a MAO molecule captures a Cl^- ion from the $Cp_2ZrClCH_3$ precursor (Eq. (2)). The heterolytic rupture of Zr–Cl bond is favored by the Lewis acidity of MAO. Two ionic species, namely, $Cp_2ZrCH_3^+$ and $MAO–CH_3Cl^-$, are produced by this reaction. The second one receives the chlorine anion. The net reaction of active ion-pair formation is attained combining these reactions as it is shown in Eq. (3). For comparison, the formation reaction of these two ionic species from the dichloride complex was also considered (Eq. (4)). Finally, notice that the balance of energy corresponding to reaction of Eq. (5) will give us the stability of active species where the ions are in direct interaction in comparison to the isolated ionic

components of catalytic site.

$$Cp_2ZrCl_2 + MAO\text{–}CH_3 \rightarrow Cp_2ZrClCH_3 + MAO\text{–}Cl \quad (1)$$

$$Cp_2ZrClCH_3 + MAO\text{–}CH_3 \rightarrow Cp_2ZrCH_3^+ \cdots MAO\text{–}CH_3Cl^- (\text{active site}) \quad (2)$$

$$Cp_2ZrCl_2 + 2MAO\text{–}CH_3 \rightarrow Cp_2ZrCH_3^+ \cdots MAOCH_3Cl^- (\text{active site}) + MAO\text{–}Cl \quad (3)$$

$$Cp_2ZrCl_2 + 2MAO\text{–}CH_3 \rightarrow Cp_2ZrCH_3^+ + MAOCH_3Cl^- + MAO\text{–}Cl \quad (4)$$

$$Cp_2ZrCH_3^+ + MAOCH_3Cl^- \rightarrow Cp_2ZrCH_3^+ \cdots MAOCH_3Cl^- (\text{active site}) \quad (5)$$

In this work the calculations will be focused firstly on Eq. (3), which can be considered the net activating process corresponding to this catalytic system. On the other hand, Eq. (4) allows us to study the isolated ionic species acting as active sites. Finally, Eq. (5) is important to evaluate the thermodynamic direction of this reaction.

2. Theoretical background

The total energy of our molecular model for the catalytic site and each of its fragments was calculated within the DFT formalism [12]. The B3LYP functional for exchange and correlation was used to take into account non-local effects of electronic density. Molecular orbitals were expanded with a gaussian basis set, namely the split valence 3–21G** basis, including polarization *p*-type functions on hydrogen atoms, *d*-type functions on C, O, Al, Cl, atoms and (*d*, *f*)-type functions on Zr atom. This was an all-electron calculation without any approximation for the core region potential, allowing to describe the influence of valence orbitals on core levels. All the calculations were performed using the GAUSSIAN'98 package [13]. The geometry of the Cp_2ZrCl_2/MAO system and of the cationic $Cp_2ZrCH_3^+$ fragment were fully optimized, while only a partial optimization was accomplished for the MAO–CH_3Cl^- counterion. The reaction energy of the catalytic site ΔE was defined like the following total energy difference:

$$\Delta E = E_T(\text{ion-pair}) + E_T(\text{MAOCl}) - E_T(\text{di-chlorozirconocene}) - 2E_T(\text{MAO–CH}_3) \quad (6)$$

Instead, we considered also the overall process from the ionic species as reactants:

$$\Delta E = E_T(\text{ion-pair}) - E_T(\text{methyl–zirconocene}^+) - E_T(\text{MAO–CH}_3\text{Cl}^-) \quad (7)$$

Atomic charges, electron transfers and molecular orbital occupations were obtained with the Natural Bond Orbital (NBO) analysis [14]. A study of orbital overlap population was also performed according to Mülliken's technique [15]. To explore the counterion approaches to zirconocene the electrostatic potential $V(r)$ and the Laplacian of electron density $\nabla^2\rho(r)$ for the isolated cation were plotted using contour graphics. Then the charge density difference $\Delta\rho(r)$ and the Laplacian $\nabla^2\rho(r)$ contour graphics were plotted for the active sites to evaluated the electronic effects of the MAO–CH_3Cl^- approximation to form the ion-pair. The $\Delta\rho(r)$ study was performed computing the difference of the electron density point to point between the ion-pair and the isolated cation complex plus the isolated MAO–CH_3Cl^- counterion.

3. Models

3.1. Zirconocene and ion-pair formation

In Fig. 1 the full optimized geometry of the isolated cation $Cp_2ZrCH_3^+$ is depicted. Due to a small methyl rotation this cation do not fulfill the requirements for the C_s symmetry group. Taking into account recent reported information two possible active species in which the MAO–CH_3Cl^- counterion forms an ion-pair were evaluated [16]. The difference between them is the way the zircocation approaches to the MAO–CH_3Cl^- counterion. One corresponds to make a close interaction with an oxygen atom of

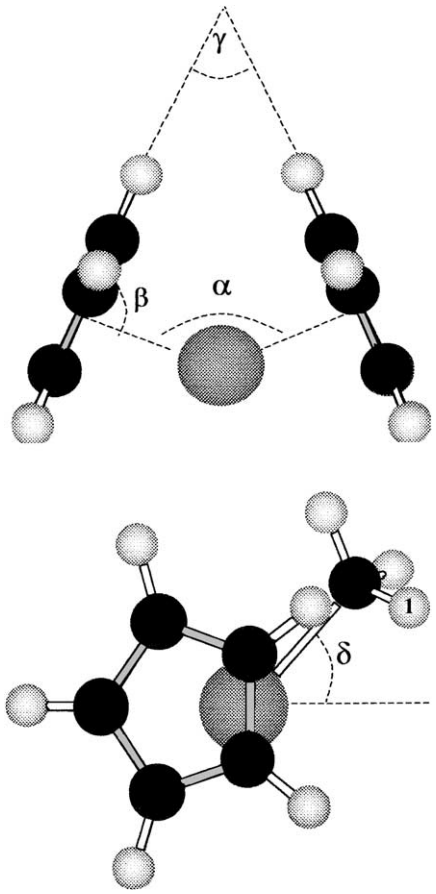

Fig. 1. Model of zircocation. This picture presents the different optimized bond angles. If necessary and for clarity, the methyl group was omitted.

$MAO–CH_3Cl^-$ and the other one to approximate the counterion through a chlorine bridge. In Section 4, a more detailed description of these approximation processes will be given.

3.2. Model of cocatalyst: MAO

In the specialized literature excellent reviews about the MAO structure have been published and here a replay of all the MAO models suggested until now will not be given. Despite the large effort made to elucidate the MAO structure in solutions, many questions remain about this subject. Recently, different hypotheses about MAO structure have been formulated from experimental evidences and well defined model compounds [17]. Actually, it is well known that the aluminum atoms are more stable in a tetrahedral than in a trigonal planar configuration due to their Lewis acid character. Therefore, O → Al dative bonds have a high tendency to be formed, producing aggregation of the chains [18]. This aggregation process results in tridimensional arranges with different shapes connected between them at dynamical equilibrium [19].

According to Ystenes et al. [20] the most probably species in MAO solution is characterized by the following general formula $(MeAlO)_9$, taking a "cage-like" structure (Fig. 2). From this and the above considerations, the MAO model proposed in this work is in relationship with the "cage" structures of these oligomers in solution. This MAO cage contains aluminum and oxygen atoms in alternative vertices forming four- or six-membered rings. Two parallels six-rings are the top and the bottom of the cage, and alternatively four- and six-membered rings form the rest of the framework. This "cage" model has a high regular symmetry (C_{3h}).

The MAO model proposed in this paper is a reduced fraction of this "cage" structure. It was imaged in order to take into account the interaction zone between metallocene and MAO. A cluster with 16 atoms constitutes this $MAO–CH_3$ model: three Al, three O, one C and nine H (Fig. 3a). Aluminum and oxygen atoms participate in two bonded four-membered

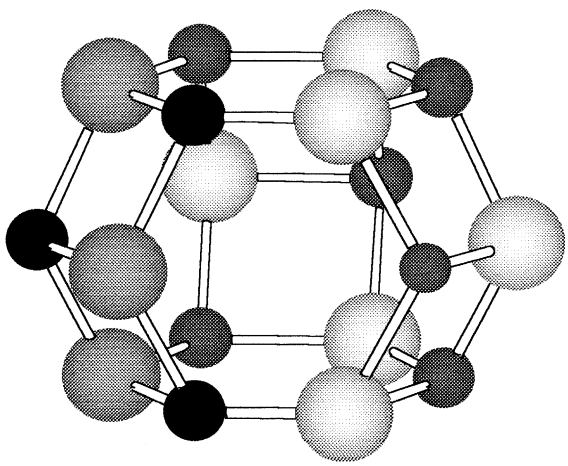

Fig. 2. The most probably "cage" species of MAO with basic formulae $(MeAlO)_9$ proposed by Ystenes et al. [20]. Darker colors of atoms show the reduced fraction of MAO used in this paper.

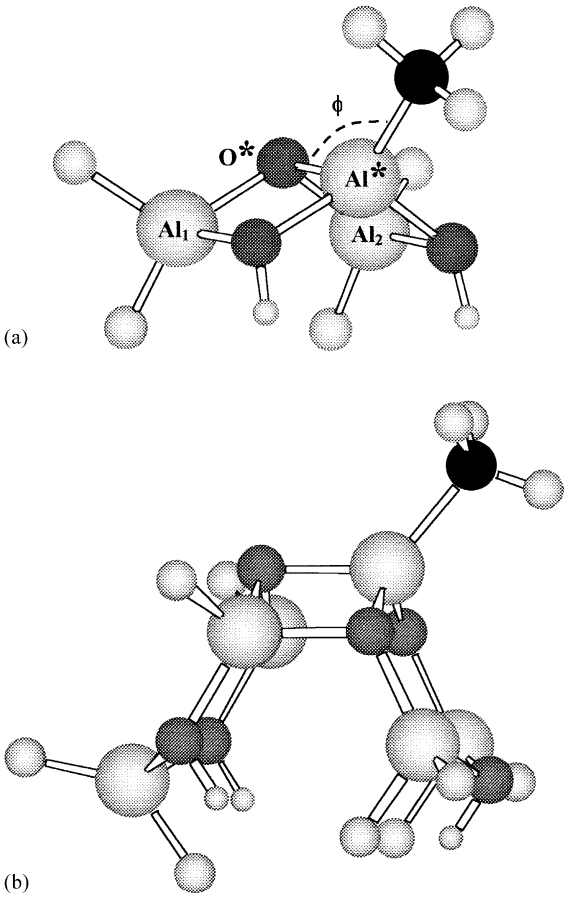

Fig. 3. (a) Lateral view of simplified MAO–CH_3 model; (b) lateral view of cage_MAO–CH_3 model.

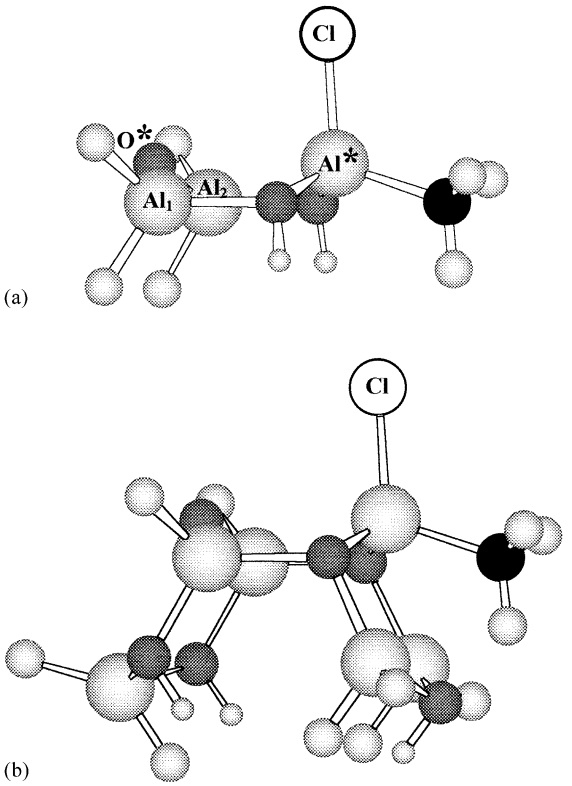

Fig. 4. (a) Lateral view of MAO–CH_3Cl^- counterion model; (b) lateral view of cage_MAOCH_3Cl^-.

rings. All the oxygen atoms are linked to aluminum atoms forming O → Al dative bonds. Therefore, all the oxygen and aluminum atoms are tri-coordinated and tetra-coordinated, respectively. This part of MAO cage should present the higher reactivity. It would be more favorable to open up O–Al bonds of four-rings than six-membered rings, due to the larger strain in smaller rings. Thus, by opening only one O → Al dative bond the strain in the two, four-rings has a high probability to be released. This situation was found in MAO–CH_3Cl^- counterion, constituted by a cluster with 17 atoms: three Al, three O, one C, nine H and one Cl (Fig. 4a).

It is a well established fact that metallocene systems need a high molar relation Al(MAO):Zr to get a productive homogeneous catalyst and relatively stable kinetic profiles (10^3–10^4 M) [21]. Due to the very small Zr concentration, one MAO molecule interacts with only one zirconocene in the active site formation step. For this reason and considering the likely proximity between the zirconocene catalyst and the MAO cocatalyst, the last was modeled only by a small part of the complete MAO molecule. Moreover, in this way the computational time was reduced without loose of information quality.

The tridimensional structure of our MAO model includes only one methyl group linked to the central Al of the two bonded four-membered rings, the other dangling bonds of Al and O atoms being saturated with six H atoms (see Fig 3a). Two of them replace two methyl groups, while the other four H saturate the coordination number of each Al and O atoms. The dangling bonds would be continued to form the six-membered rings of the MAO cage. The procedure of saturation with H atoms has been widely used in the past for

different systems to eliminate spurious effects due to these unsaturated dangling bonds [8,22].

Due to fact that the MAO model is a fraction of a bigger MAO structure some bond angles have been taken as fixed to simulate the entire tridimensional cage of MAO. In case of MAO–CH_3 and MAO–CH_3Cl^- clusters the terminal bond angles, i.e. those corresponding to the cage MAO structure and those saturated with H, were taken as frozen. However, the H atoms that replace two methyl groups were left free. For MAO–CH_3, the optimization process does not produce the rupture of Al*–O* central dative bond. A strong interaction between internal Al and O atoms is obtained, forming two cycles of four-members each one. On the other hand, the geometrical optimization for MAO–CH_3Cl^- produces an opening of the previous mentioned bond due to the Cl^- presence.

In order to evaluate the influence of cluster size in our calculations based on models previously described, greater clusters were considered. More precisely, the MAO–CH_3 and MAO–CH_3Cl^- clusters of Figs. 3a and 4a were extended according to the model of Fig. 2, including now three Al and O atoms. The greater MAO–CH_3 cluster is constituted by 27 atoms: 6 Al, 6 O, 1 C, 14 H and was named cage_MAO–CH_3. The greater MAO–CH_3Cl^- cluster is similar, besides the Cl extra atom, and was named cage_MAO–CH_3Cl^- (see Figs. 3b and 4b, respectively). Following the same procedure outlined for the smaller clusters the dangling bonds were saturated with H atoms in order to have a complete coordination for each terminal atom.

The fundamental aim of this work was to study the interaction between the zirconocene and cocatalyst, which is the vital part of the active site. Hence, we do not intent to optimize the more probable MAO species in solution. Instead, we decided to adopt for the MAO structure the minimal model in agreement with other experimental and theoretical data, making less expensive the calculation for the ion-pair interaction.

4. Results and discussion

4.1. Cationic complex ($Cp_2ZrCH_3^+$)

The optimized structure of cation complex is in good or very good agreement with X-ray results obtained for other cation complexes like [1,2-Me_2–Cp]$_2$Zr$CH_3^+ \cdots CH_3B(C_5F_5)_3^-$ [23] and [Me_5–Cp]$_2$Zr$CH_3^+ \cdots CH_3B(C_5F_5)_3^-$ [9] (Fig. 1). Looking the data summarized in Table 1 we observe that the Zr–C_{me} distance is in between experimental values of above both systems (2.22–2.25 Å). For the average Zr–C(Cp) distance a value of 2.522 Å is obtained, whereas the experimental value is 2.525 Å [23]. The calculated Centroid-Zr-Centroid (Centr-Zr-Centr) angle α (135.7°) is somewhat higher than experimental value (132.5°) [23]. The methyl group is bent away from the Centr-Zr-Centr plane. The calculated bending angle is slightly higher (by 11%) than that obtained by Woo et al. [9] using DFT calculations. The difference can be due to the Zr position between the Cp rings. The another bond angles are important to define the final cation structure.

Table 1
Important optimized parameters of cationic complex

Parameter	Optimized parameter[a]
Zr-Centr	2.22
Zr-C_{me}	2.24
C_{me}–H	1.09
Centr-Zr-Centr angle (α)	135.7
β	89.8
γ	54.2
δ	50.8
Zr–C_α–H_1 angle	104
Zr–H_1	2.72
Zr–$H_{2,3}$	2.87

[a] Distances expressed in Armstrong (Å) and bond angles in degrees (°).

The geometry of the isolated cation was fully optimized without any constraints or symmetry conditions. This is the reason why a significant α-agostic interaction is obtained, in comparison with Woo results. This observation is evidenced by the relatively less opened Zr–C_α–H angle (104°) and the concomitant small Zr–H distance, in comparison with the other Hs of the CH_3 group (see Table 1). In addition, the Cp rings present an eclipsed conformation in agreement with other calculations, showing that this is the most stable cation conformation in the initial state [5c].

The possible counterion approaches to zirconocene were firstly studied by mapping the electrostatic potential distribution $V(r)$ of cation complex $Cp_2ZrCH_3^+$. From an adequate grid of points we were able to

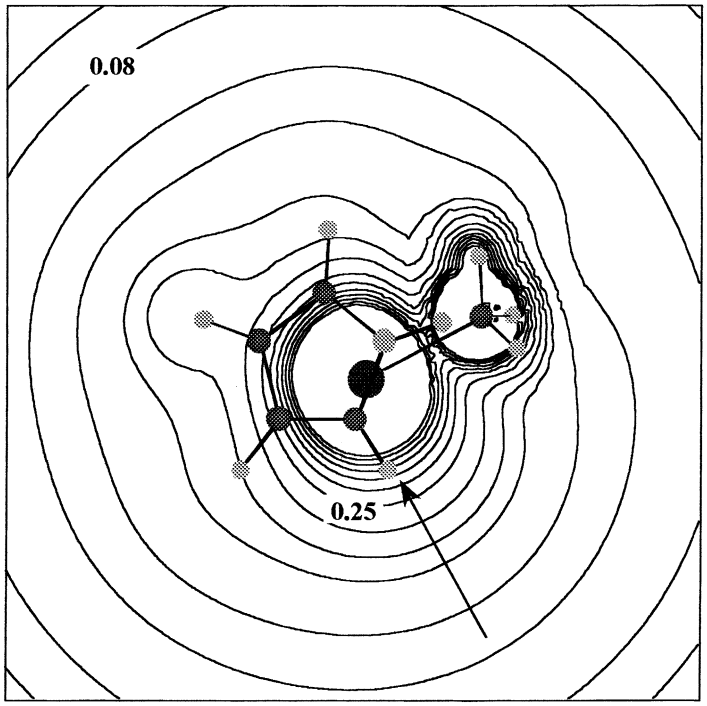

Fig. 5. Electrostatic potential $\Phi(r)$ corresponding to cation complex $Cp_2ZrCH_3^+$. Contour map along the Zr–C_{me} plane. Electrostatic potentials are expressed in a.u.

define the plane containing the desire interaction region (see Fig. 5). Notice that the entire potential map is positive due to the net positive charge of cation. This positive potential increases abruptly near the core of Zr and C atoms. However, the approaching zone of the MAO-CH_3Cl^- counterion to the Zr cation likely should be localized in the valence electron cloud where the potential gradient is higher, i.e. where the electrostatic attraction on the anion is stronger. An arrow in Fig. 5 shows the most probably interaction zone between cation and counterion, excepting the regions around the $–CH_3$ group and the Cp ligands. Both previous mentioned zones present important steric hindrances. Similar theoretical results were obtained with DFT calculations for the cation complex $Cp_2Zr–^nPr^+$ [24], which define the most probably zone for an ethylene molecule to approach the catalytic site.

Looking now at the Laplacian distribution, it is possible to show the regions with high ($\nabla^2\rho(r) < 0$) and low ($\nabla^2\rho(r) > 0$) electron charge concentration (see Fig. 6a). The highest charge concentration is around the Zr and C_{me} atoms (broken lines), along the covalent Zr–C bond. The depletion of charge (solid lines) presents a channel near the Zr atom, indicating the better way where the MAO–CH_3Cl^- counterion could approach to cation complex. This is displayed by the arrow of the Fig. 6a. The $\nabla^2\rho(r)$ profile along a line beginning in the Zr atom shows this property (Fig. 6b). Both results, electrostatic potential and Laplacian distribution, give the same kind of information.

4.2. MAO models

Taking into account our previous considerations, the bond distances and bond angles were optimized, including the geometry of the methyl conformer of the initial species of MAO. Besides, an additional study was performed, adding a Cl anion in MAO to form a MAO–CH_3Cl^- counterion (Fig 4a). It is well known the X^- anion abstraction ability of MAO (X: halogen or alkyl group) from a neutral metallocene [25]. The optimized parameters for both species are presented in Table 2. The more substantial change in

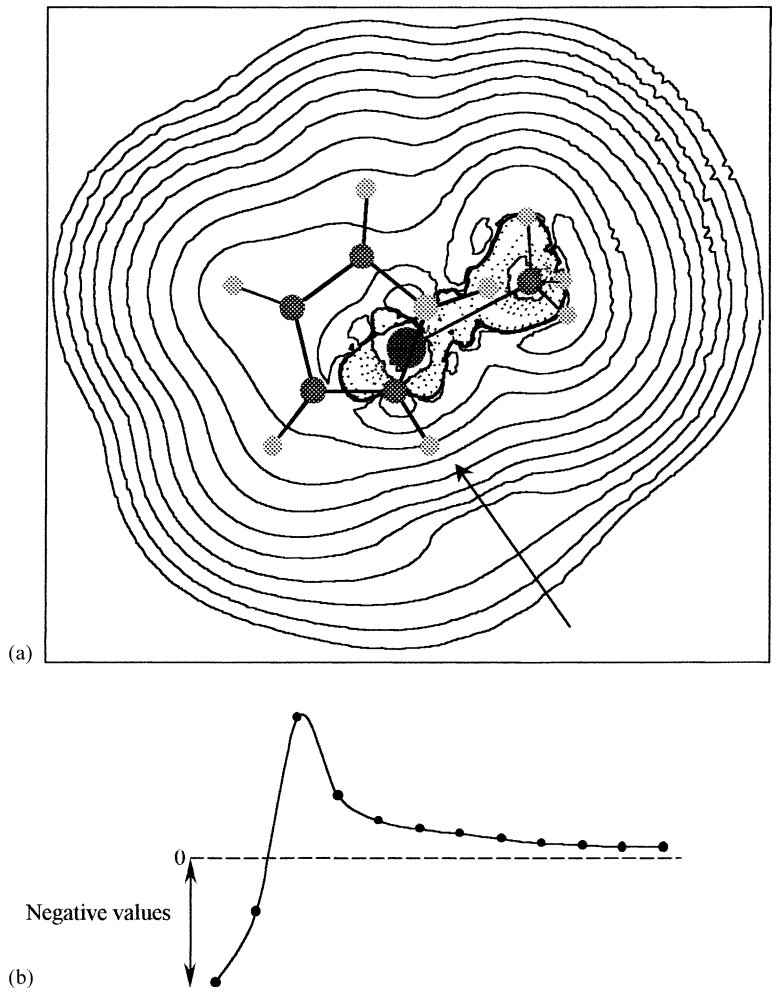

Fig. 6. (a) Laplacian $\nabla^2\rho(r)$ distribution of charge density. Contour map is along the Zr–C_{me} plane. Solid lines are for $\nabla^2\rho > 0$ (regions of charge depletion); broken lines are for $\nabla^2\rho < 0$ (regions of charge concentration). The arrow indicates the most probably zone of approaches the MAO–CH_3Cl^- counterion. (b) Profile along the axis of arrow. Note the variation of charge.

bond distances occurs in O*–Al* dative bond. Looking at the values of O*–Al bonds we observe that the stretching of O* → Al* central bond is accompanied with a shortening in the others O*–Al bonds, producing a noticeably change of coordination of O* atom. Furthermore, all the internal bond angles of the ring increases from 90 to 110–120°. The arrangement of the MAO–CH_3Cl^- counterion is changed with respect the initial MAO structure. The Natural Bond Orbital (NBO) charges show the MAO–CH_3Cl^- ability to disperse the negative charge given by Cl^- (Table 3). The most important fraction of this charge is concentrated on chlorine atom, which is bonded to Al*. The rest of negative charge is distributed fundamentally on the aluminum atoms forming the MAO–CH_3Cl^- counterion. These results are in agreement with several reports related to the ability of MAO to delocalize the negative charge when acts as counterion [26].

In Table 3 the NBO atomic charges for selected atoms of cage_MAO-CH_3 and cage_MAO–CH_3Cl clusters are summarized. For the first cluster, notice a general 10–20% increase of absolute values of Al and O charges, with the exception of Al and O*, for which the charge modification is negligible. In addition, the

Table 2
Distance and angle bonds optimized in MAO–CH_3 and MAO–CH_3Cl^- counterion models

Parameter	Optimized parameter[a]	
	MAO–CH_3	MAO–CH_3Cl^-
O*–Al* distance	1.83	3.02
Al*–O distance	1.82	1.81
O*–Al distance	1.84	1.74
Al*–C_{me} distance	1.92	1.96
Al*–Cl distance	–	2.12
Al–H distance	1.61	1.65
O–H distance	0.98	0.98
O–Al–C_{me} angle (ϕ)	129.1	102.7
Cl–Al–C_{me} angle	–	112.4
O–Al–O angle	90	110/120

[a] Distances are given in Armstrong (Å) and bond angles in degrees (°).

atomic charges are more homogeneously distributed than in the MAO–CH_3 cluster. A very similar behavior is observed for the cage_MAO–CH_3Cl cluster. Looking at the overall distribution of electronic charge we notice that the negative charge coming from chlorine anion is re-distributed over all the atoms of greater cluster.

In Table 4 the overlap population (OP) and electron transfers of NBO for MAO–CH_3 and MAO–CH_3Cl clusters are summarized. We observe that the central O* → Al* bond becomes the most probably bond to be broken with chloride addition. The OP for this oxygen atom is the lowest. On the other hand, the OP's for the others O*–Al bonds are higher in MAO–CH_3Cl^- species. Analogous OP results, not shown here, were obtained for cage_MAO–CH_3 and cage_MAO–CH_3Cl cluster species. This fact can be related to the strength of these bonds when Cl^- is added. Besides, two slightly electron transfers occur between donor lone pair of oxygen and accepting two anti-bonding orbitals in MAO–CH_3Cl^-. Note that the broken O* → Al* central bond produces a redistribution of electron charge. Thus the O* can be view actually as a di-coordinated oxygen. These electron transfers in the MAO–CH_3Cl^- molecule are in agreement with the lower negative charge on di-coordinated oxygen reported in Table 3. Nevertheless, they do not take place in MAO species.

Table 4
Overlap Population and NBO electron transfer energetic parameter corresponding to MAO–CH_3 and MAO–CH_3Cl^- species

Dative bond	Overlap population	
	MAO–CH_3	MAO–CH_3Cl^-
O* → Al*	0.192	0.036
O* → Al_1	0.238	0.336
O* → Al_2	0.243	0.338
Electron transfer: donor NBO → acceptor NBO	Energy (kcal/mol)	
	MAO–CH_3	MAO–CH_3Cl^-
n O* → π* (O–Al_1)[a]	–	11.91
n O* → π* (O–Al_2)	–	11.86

[a] "n" stands for a lone pair of O*.

4.3. Ion-pair formation

In a previous work it was considered the possibility of existence two counterion agents (MAOCl$^-$

Table 3
Natural bond orbital (NBO) charge analysis of the principal atoms of MAO–CH_3 and MAO–CH_3Cl^- counterion

Atom	MAO–CH_3 (a.u.)	MAO–CH_3Cl^- (a.u.)	Cage MAO–CH_3 (a.u.)	Cage MAO–CH_3Cl^- (a.u.)
Al*	1.73	1.63	1.73	1.58
Al	1.23	1.15	1.52	1.49
Al	1.23	1.15	1.52	1.49
O*	−1.13	−1.07	−1.15	−1.12
O	−1.02	−1.00	−1.14	−1.11
O	−1.00	−1.02	−1.12	−1.14
Cl	–	−0.56	–	−0.57
C	−1.33	−1.31	−1.34	−1.39
H	0.25	0.21	0.26	0.26
H	0.26	0.23	0.26	0.25
H	0.26	0.23	0.26	0.26

Cl atom is bonded with Al*. Atomic charges of cage_MAO–CH_3 and cage_MAO–CH_3Cl^- were included.

and $MAOCl_2^-$) [16d]. However, the MAOCl cocatalysts necessary to generate the $MAOCl_2^-$ counterion are present in very low concentration with respect to MAO species. For this reason, we studied here the mono-chlorine counterion. The possible MAO–CH_3Cl^- approaches to zircocation were proposed appealing to previous information extracted from open literature [8,16a,16b,16d,27,28]. Barron and co-workers [16b] found that, in case of aluminoxane clusters, such as $(^t Bu)_6Al_6(\mu_3O)_6$, three-coordinated aluminum is not a prerequisite for ethylene polymerization activity when combined with zirconocene dimethyl. According to their ^{1}H-NMR results, the cage species of aluminoxane react exothermically with Cp_2ZrMe_2 at room temperature to produce an ethylene polymerization-active tightly ion-paired species $Cp_2ZrMe\cdots(^t Bu)_6Al_6(\mu_3O)_6Me$. From the point of view of these authors the driving force for the abstraction of CH_3^- is assumed to be the "latent Lewis acidity" produced by the ring strain present in the small rings. Here, taking into account our previous considerations, the ion-pair formation was evaluated assuming two different approaches of the MAO–CH_3Cl^- counterion to cation complex: close interaction Zr–O* (Site 1) (Fig. 7) and interaction through a chlorine bridge from MAO–CH_3Cl^- (Site 2) (Fig. 8).

The more relevant parameters for these sites are summarized in Table 5. The results indicate that both MAO–CH_3Cl^- approaches produce negligible changes in the Zr–C_{me} distances with respect to the isolated cation complex. On the other hand, the δ angle of methyl group varies significantly. An important

Table 5
Optimized distance and angle bonds obtained from $Cp_2ZrCH_3^+\cdots$ MAO–CH_3Cl^- for both type of sites

Parameter	Optimized parameter[a]	
	Site 1	Site 2
Zr–Cl distance	3.73	2.58
Zr–O* distance	2.95	5.43
Zr–C_{me} distance	2.27	2.26
ϕ Angle (Figs. 8 and 9)	73.7	102.2
δ Angle (Fig. 1)	62.0	53.7
Al*–Cl distance	2.12	2.20

[a] Distances are given in Armstrong (Å) and bond angles in degrees (°).

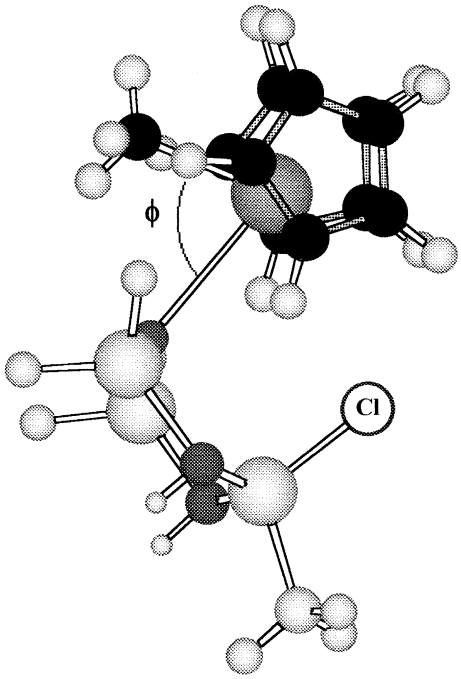

Fig. 7. Optimized geometry of Site 1.

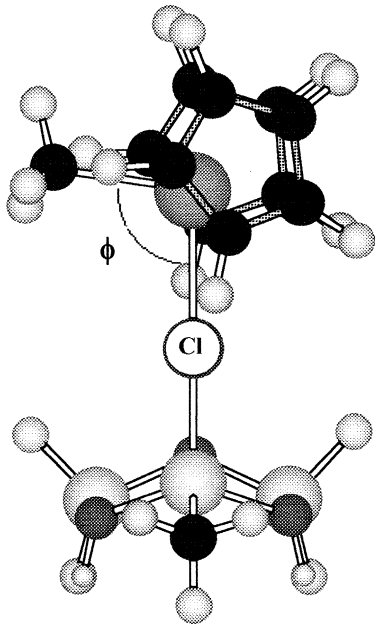

Fig. 8. Optimized geometry of Site 2.

increase is observed in Site 1. The sites present noticeably differences in geometry. In case of Site 1 the O* of MAO–CH_3Cl^- is closer to Zr atom than the Cl by 1.1 Å. In case of Site 2 the situation is inverted; the Cl of MAO–CH_3Cl^- becomes the closest. Although the Zr–Cl distance for Site 2 is relatively shorter than the Zr–O* distance for Site 1 (by 0.3 Å), the Zr–O* distance for Site 2 is remarkably longer than the Zr–Cl distance for Site 1 (by 1.7 Å). This fact shows us that the best interaction between cation complex and counterion (contact ion-pair) would be expected for Site 1. In other words, this site presents a close contact ion-pair while Site 2 has a loosened contact ion-pair, giving a more opened active site. Another parameter to represent the different approaches is the ϕ angle. The more open angle is obtained for Site 2. In both cases our results are in general agreement with those obtained by electrostatic potential $V(r)$ and $\nabla^2\rho(r)$ mapping for isolated cation. The most probably zone for a MAO–CH_3Cl^- approach was correctly predicted by the previous mentioned analysis.

It is a well established fact that dichloride catalyst and cocatalyst must interact to produce the active site. In the present work the different processes that give Site 1 and Site 2 were analyzed considering the reaction energies as defined in Eqs. (3)–(5). First, the reaction was evaluated assuming the presence of two cocatalyst molecules to form the active species. The Cp_2ZrCl_2 catalyst was modeled taking into account recent references of its geometry (distances and angles not shown here) [29]. The reaction energies (ΔE) for the ion-pair formation were evaluated using Eq. (3) and are summarized in Table 6. The results of first and second entries in Table 6 clearly indicate the effective formation of the sites when the counterion is included, being both processes exothermic. Moreover, when only the isolated component species $Cp_2ZrCH_3^+$ and MAO–CH_3Cl^- are produced (third entry), the energy computed using Eq. (4) reduces significantly.

Second, we considered that the active sites could be produced directly from $Cp_2ZrCH_3^+$ and MAO–CH_3Cl^- according to the Eq. (5). The reaction energies calculated using this equation (fourth and fifth entries of Table 6) show also that both cation–anion ion-pairs present high stability with respect to the ion species, assuring the presence of ion-pair as active sites. Notice that the production of Site 1 is nearly 20 kcal/mol higher exothermic than Site 2. The main difference between both active sites is the degree of interaction between zircocation and counterion. Effectively, the link between zirconium of $Cp_2ZrCH_3^+$ and oxygen of MAO–CH_3Cl^- in Site 1 is higher polarized in the local interaction zone than the link in Site 2, making less probable the participation of isolated ionic species as active sites (see later charge analysis).

In third column of Table 6 are summarized the reaction energy values obtained with greater clusters. Here only single point calculations were performed for both active sites, maintaining the optimized geometries corresponding to the smaller MAO–CH_3Cl^- counterion. It is clear that not significant changes are produced. Therefore, at least from an energetic point of view, the results obtained with smaller clusters can be taken as valid in order to define trends and make relative comparisons. We underline that these reaction energies are dependent on the MAO region where reaction take place, independently of the size of the model.

The NBO charges in Table 7 show the change of charge distribution when the ion-pairs are formed for both counterions MAO–CH_3Cl^- and cage_MAOCH_3Cl^-. If the charges of isolated species, cation and counterion are compared the

Table 6
Reaction Energies of $Cp_2ZrCH_3^+\cdots$ MAO–CH_3Cl^- and $Cp_2ZrCH_3^+\cdots$ cage_MAO–CH_3Cl^- for both types of sites

Reaction	ΔE (kcal/mol)	ΔE with MAO cage (kcal/mol)
$Cp_2ZrCl_2 + 2$ MAO–$CH_3 \rightarrow Cp_2ZrCH_3^+\cdots(\mu_1O^*)$ MAO–CH_3Cl^- (Site 1) + MAO–Cl	−293.45	−296.19
$Cp_2ZrCl_2 + 2$ MAO–$CH_3 \rightarrow Cp_2ZrCH_3^+\cdots(\mu_1Cl)$ MAO–CH_3Cl^- (Site 2) + MAO–Cl	−272.66	−272.60
$Cp_2ZrCl_2 + 2$ MAO–$CH_3 \rightarrow Cp_2ZrCH_3^+ +$ MAO–CH_3Cl^- + MAO–Cl	−176.17	−178.17
$Cp_2ZrCH_3^+ +$ MAO–$CH_3Cl^- \rightarrow Cp_2ZrCH_3^+\cdots(\mu_1O^*)$ MAO–CH_3Cl^- (Site 1)	−117.26	−118.01
$Cp_2ZrCH_3^+ +$ MAO–$CH_3Cl^- \rightarrow Cp_2ZrCH_3^+\cdots(\mu_1Cl)$ MAO–CH_3^- (Site 2)	−96.48	−94.43

Table 7
NBO charge analysis of $Cp_2ZrCH_3^+ \cdots MAO–CH_3Cl^-$ and $Cp_2ZrCH_3^+ \cdots$ cage_MAO–CH_3Cl^- for both types of sites

Atoms and species	MAO–CH_3Cl^- [a]	Cp_2ZrCl_2	$Cp_2ZrCH_3^+$	Site 1	Site 2	Site 1_cage	Site 2_cage
Zr	–	1.07	1.65	1.67	1.38	1.69	1.38
Cp_1	–	−0.20	−0.15	−0.30	−0.21	−0.28	−0.20
Cp_2	–	−0.20	−0.15	−0.31	−0.14	−0.29	−0.15
$Cp_2ZrCH_3^+$	–	–	1	0.64	0.64	0.69	0.65
Cl	−0.56	−0.34	–	−0.50	−0.38	−0.50	−0.37
O*	−1.07	–	–	−1.04	−1.07	−1.10	−1.13
Al*	1.63	–	–	1.65	1.69	1.58	1.62
Al	1.15	–	–	1.22	1.13	1.55	1.49
Al	1.15	–	–	1.22	1.14	1.57	1.49
MAO–CH_3Cl^-	−1	–	–	−0.64	−0.64	−0.69	−0.65

The comparison was accomplished taking into account the Cp_2ZrCl_2 catalyst and the isolated cation and MAO–CH_3Cl^- counterion.
[a] Charges are expressed in atomic units (a.u.).

MAO–CH_3Cl^- looses negative charge (∼0.36 *e*) which it is transfer to cation complex. This result is accompanied with a concomitant gain of negative charge of zircocation. For both active sites the net charges of cation and counterion are the same. However, the redistribution of the charge is different depending of the active species. In case of Site 1 the Zr atom preserves its positive value, but the Cp ligands increase up to 100% the negative charge. For Site 2 the gained negative charge in cation complex is preferentially located in Zr atom. Besides, the Cp charges are noticeably affected by the position of the MAO–CH_3Cl^- in this site. Only the Cp ligand more distant from the MAO–CH_3Cl^- counterion increases up to 50% its negative charge. In case of isolated cation complex the Cp charges are equal, indicating similar electron transfer to Zr atom for both Cp ligands and vice versa. The same behavior occurs in Site 1. Nevertheless, this situation does not occur for Site 2. The positive charge transferred to the MAO–CH_3Cl^- counterion is distributed rather homogeneously on the ring for Site 1, while it is received fundamentally by the Cl atom for Site 2. We can say that the MAO–CH_3Cl^- counterion forming the Site 2 undergoes a polarization due to the interaction with cation trough Cl bridge. The Cl atom releases negative charge which is localized in the two neighbour aluminum atoms.

The charge distributions on sites where the cocatalyst is represented by cage_MAO–CH_3Cl^- are very similar to those obtained with the smaller cluster. Particularly, the charge of the Zr ion is almost the same. The main differences are observed in the counterion, specially for O and Al atoms, as it was commented above for the cage_MAO models alone in Section 4.2. Therefore, a cluster containing only the immediate atoms in the interaction region around the cation is a sufficiently good model to study the influence of cocatalyst. By this reason in the following we will restrain to use the smaller size models.

In Table 8 are summarized the main charge transfers taking place in the ion-pair expressed in terms of the NBO analysis. First we analyze those between Cp rings and Zr, and vice versa. Due to the aromatic character of Cp ligands the charge transfers involve the two C=C bonds (σ and π) and one C lone pair of these ligands. Notice the important electron transfers obtained for $Cp_2ZrCH_3^+$ as the third and fourth columns in Table 8 show. The position of the MAO–CH_3Cl^- counterion produces different electron transfers to/from the zircocation. For Site 1, the net electron transfers from Cp towards Zr atom decrease with respect to the isolated cation. These results are compatible with NBO values of atomic net charges of Cp rings of Site 1, which are more negative. In case of Site 2, it presents a greater net electron transfer from Cp towards Zr atom in comparison with Site 1 and the atomic net charges of Cp rings are less negative. The Zr charge receives also contributions from MAO–CH_3Cl^-. Notice the much important transfer from Cl in the case of Site 2 than the transfer from O* in Site 1, making the Zr relatively much positive in the last case. Taking into account this NBO analysis, Site 2 in comparison with Site 1 presents poor polarization in cation complex and higher polarization in

Table 8
The most important electron transfer parameters obtained by NBO analysis for the isolated cation complex, Sites 1 and 2

Transfers	Donor NBO → acceptor NBO	$Cp_2ZrCH_3^+$[a]		Site 1[a]		Site 2[a]	
		Cp_1	Cp_2	Cp_1	Cp_2	Cp_1	Cp_2
$Cp_{1,2} \rightarrow Zr$	$\Sigma\sigma$ (C–C) → n Zr	51.03	50.44	86.87	72.78	129.61	63.93
	$\Sigma\pi$ (C–C) → n Zr	99.01	96.95	50.06	37.60	63.74	126.23
	n C → n Zr	94.84	93.91	54.84	78.48	77.78	83.23
$Zr \rightarrow Cp_{1,2}$	n Zr → $\Sigma\pi^*$ (C–C)	97.93	78.13	109.68	60.24	58.85	50.42
$O^* \rightarrow Zr$	n O^* → n^* Zr	–		51.80		–	
$Cl \rightarrow Zr$	n Cl → n^* Zr	–		–		135.88	

[a] Energy expressed in kcal/mol.

$MAO–CH_3Cl^-$ counterion: the Zr atom has low positive charge and the Cp ligands small negative charges. Otherwise, for Site 1 the Zr atom is more positive and the Cp rings more negative.

The computation of charge density difference $\Delta\rho(r)$ over a specific plane of a molecule shows the gain or loose of electron charge. Here, the Centr-Zr-Centr plane was selected for this analysis. Figs. 9 and 10 show positive values of $\Delta\rho(r)$ in the Cp zones, indicating an electron density gain when the cation and counterion are near each other (ion-pair). In case of Site 2, we obtain complex contour plots due to the asymmetry of the active sites. However, the most important zones to highlight are localized between Zr and Cp rings. The graph shows negative values of $\Delta\rho(r)$ in almost all the region between the Cp rings. Nevertheless, a positive branch connects one Cp ligand with Zr atom indicating an electron density gain between this Cp ring and Zr. These results are in agreement with those obtained by NBO analysis. In active Site 2 the Zr atom and Cp_1 ligand are the dominant acceptors of the electron charge of $MAO–CH_3Cl^-$; the charge in the $MAO–CH_3Cl^-$ is distributed as looser as possible in the cation complex. On the other hand, in Site 1 the electron charge is localized symmetrically all around of Zr atom.

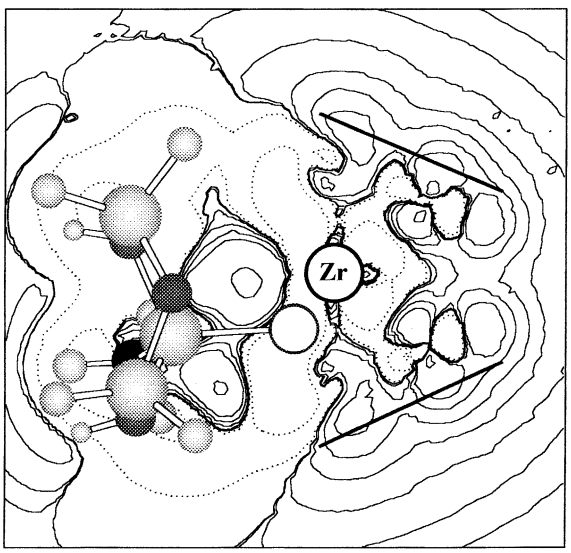

Fig. 9. Charge density difference $\Delta\rho(r)$ for Site 1 ion-pair. Contour plot along the Centr-Zr-Centr plane. Dotted lines correspond to $\Delta\rho < 0$ and solid lines refer to $\Delta\rho > 0$. Dark lines (Cp ligands) and Zr atom were sketched in the picture for better comprehension.

The Laplacian of density $\nabla^2\rho(r)$ was evaluated for both active sites. Different planes were selected to plot the contour lines. In case of Site 1 we considered a cross section containing Zr–C_{me} and Zr–O^* bonds (Fig. 11). The Laplacian results can express the different type of bonds contained in that plane. The $\nabla^2\rho(r)$ is negative in the Zr–C_{me} bond zone (dotted lines). On the other hand, the $\nabla^2\rho(r)$ is positive through Zr–O^* bond (solid lines). The negative values of the $\nabla^2\rho(r)$ between Zr and C_{me} show an important charge electron accumulation in the zone bond and they are an evidence of a covalent bond. Otherwise, the positive values of the $\nabla^2\rho(r)$ between Zr and O^* correspond to an electron depletion in the interaction zone, and constitute an evidence of an ionic bond. In this case, the charge density is concentrated towards the atoms instead in the bond zone. In the same figure is possible to observe the Al^*–Cl bond, which show characteristics of an ionic bond. A similar analysis was performed on Site 2. In this case, the selected cross section contains Zr–C_{me} and Zr–Cl bonds

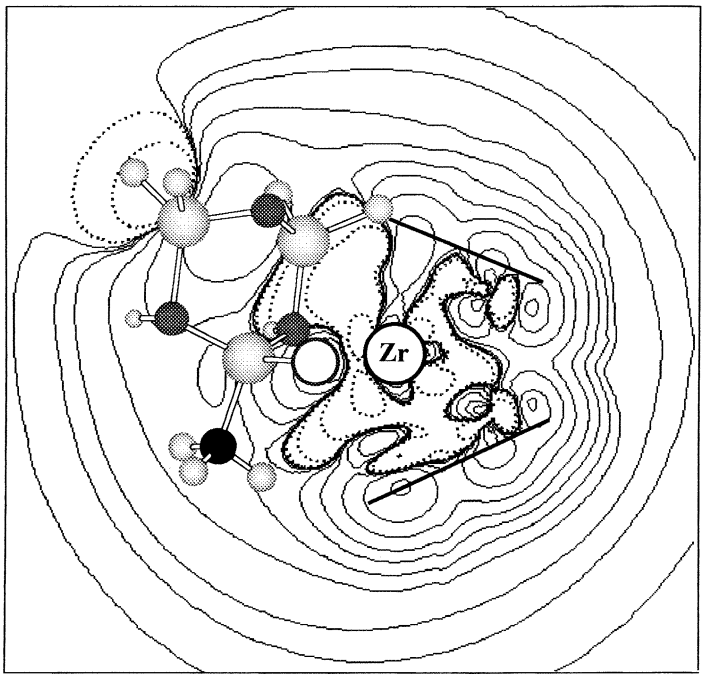

Fig. 10. Charge density difference $\Delta\rho(r)$ for Site 2 ion-pair. Contour plot along the Centr-Zr-Centr plane. For caption details see Fig. 9.

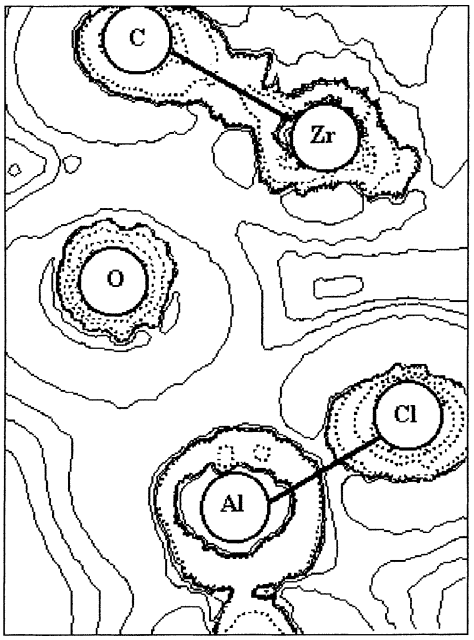

Fig. 11. Laplacian $\nabla^2\rho(r)$ distribution of charge density for Site 1. Contour map thorough Zr–C_{me} bond (from cation), O* and Al*–Cl bond (from MAO–CH_3Cl^-) (Fig. 7). For details see caption of Fig. 5.

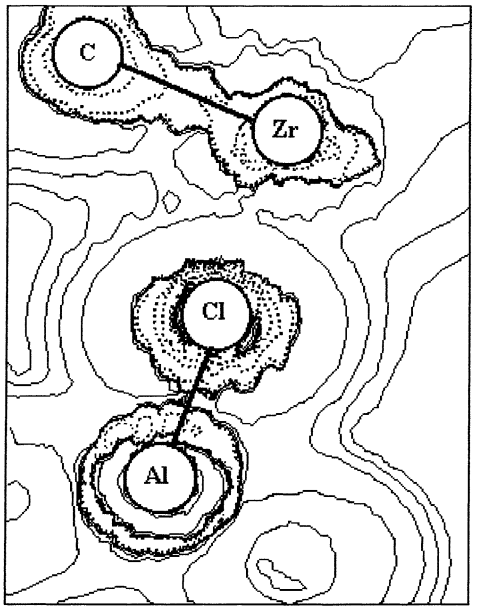

Fig. 12. Laplacian $\nabla^2\rho(r)$ distribution of charge density for Site 2. Contour map thorough Zr–C_{me} bond (from cation) and Al*–Cl (from MAO–CH_3Cl^-) bond (Fig. 8). For details see caption of Fig. 5.

(see Fig. 12). Again, the Laplacian of density is positive between Zr and Cl atoms, indicating an ionic bond. The Zr–C_{me} is maintained as covalent bond. This analysis of the Laplacian was proposed by Bader et al. [30] for other species. Actually, it is a helpful tool that was used in many recent reports [31].

5. Conclusion

The Cp_2ZrCl_2/MAO interaction as an ion-pair, including the counterion, was studied theoretically using a self-consistent molecular orbital DFT method and a molecular model for MAO. The analysis of results was focused on the electronic structure of possible $Cp_2ZrCH_3^+ \cdots MAO–CH_3Cl^-$ ion-pairs. Two different approaches of the $MAO–CH_3Cl^-$ counterion to cation complex were considered. The reaction energy results indicate the ion-pair formation as active species instead of isolated cation and counterion. Both active sites are stable complexes. The cluster size effect on $MAO–CH_3$ and $MAO–CH_3Cl^-$ models was evaluated. The results showed that our small clusters are able to predict the more relevant energetic and electronic properties coming from the direct interaction in the ionic pair species.

In particular, a redistribution of charge is produced when the counterion approaches to the cation. The closeness of $MAO–CH_3Cl^-$ counterion produces an electron donation to the zircocation. The two ion-pairs considered present the same net charges in cation complex and counterion, but with a completely different redistribution. Site 1 takes the most significant negative charge in Cp rings while in Site 2 the charge is localized preferentially in Zr atom and in the looser Cp, with respect to the counterion. The redistribution of the charge is clearly shown in charge density difference $\Delta\rho(r)$ results, where the electron density of the cation complex and counterion together and away each other are analyzed. An increase of $\Delta\rho(r)$ indicates more negative charge in Cp zones, especially in Site 1, and the connecting positive zone between Zr atom and Cp. From Laplacian $\nabla^2\rho(r)$ results is possible to confirm the ionic character of both catalytic sites. The Zr–O* bond in Site 1 and the Zr–Cl bond in Site 2 present positive $\nabla^2\rho(r)$ in the bond zones.

It is really important to take into account the presence of cocatalyst in the active site models. The approaches of $MAO–CH_3Cl^-$ toward the cation complex produce a steric constrain and a modification of net charge of zircocation. This net charge would be +1 if the analysis would be accomplished on an isolated cation (like it is normally considered in the literature when the active site is modeled). Furthermore, the cation–counterion interaction produces charge redistribution in all the atoms of the ion-pair.

Acknowledgements

We acknowledge the Consejo Nacional de Investigaciones Científicas y Técnicas (CONICET) and the Universidad Nacional del Sur (UNS) for their financial support. We want thank Dr. Daniel E. Damiani for the discussion of the experimental results related to this work.

References

[1] G. Guerra, P. Longo, L. Cavallo, P. Corradini, L. Resconi, J. Am. Chem. Soc. 119 (1997) 4394.
[2] F. Grisi, P. Longo, A. Zambelli, J.A. Ewen, J. Mol. Catal. A: Chem. 140 (1999) 225.
[3] H. Sinn, W. Kaminsky (Eds.), Hamburger Makromolekules Kolloquiom 1994, Hamnburg, Germany, 1994.
[4] K. Angermund, A. Hamuschik, M. Nolte, in: G. Fink, R. Mülhaupt, H.H. Brintzinger (Eds.), Ziegler Catalysts, Springer, Berlin, 1995, p. 251.
[5] (a) R.J. Meier, G.H.J. vanDormemaele, S. Iarloti, F. Buda, J. Am. Chem. Soc. 116 (1994) 7274;
(b) M. Toto, L. Cavallo, P. Corradini, G. Moscardi, L. Resconi, G. Guerra, Macromolecule 31 (1998) 3431;
(c) L. Petitjean, D. Pattou, M.F. Ruiz-López, J. Phys. Chem. B 103 (1999) 27;
(d) P.J. Chirik, J.E. Bercaw, Polym. Preprints 41 (2000) 393;
(e) L. Cavallo, P. Corradini, F. Grisi, P. Longo, G. Guerra, Polym. Preprints 41 (2000) 395.
[6] R. Fusco, S. Spera, L. Longo, A. Proto, L. Abis, P. Accomazzi, L. Gila, A. Guarini, S. Bertoni, C. Busetto, F. Garbassi, in: Proceedings of the Second International Congress on Metallocene Polymers, Düsseldorf, Germany, March 1996, p. 335.
[7] R. Fusco, L. Longo, F. Masi, F. Garbassi, Macromol. Rapid Commun. 18 (1997) 433.
[8] R. Fusco, L. Longo, F. Masi, F. Garbassi, Macromolecule 30 (1997) 7673.
[9] T.K. Woo, L. Fan, T. Ziegler, in: G. Fink, R. Mülhaupt, H.H. Brintzinger (Eds.), Ziegler Catalysts, Springer, Berlin, 1995, p. 292.
[10] W. Kaminsky, R. Engehausen, K. Zoumis, W. Spaleck, J. Rohrmann, Makromol. Chem. 193 (1992) 1643.

[11] I. Kim, G.N. Hwang, J. Mass Spectrom. Pure Appl. Chem. A 35 (12) (1998) 1987.
[12] (a) W. Kohn, L. Sham, Phys. Rev. 140 (1965) A1133;
(b) The challenge of d and f electrons, D.R. Salahub, M.C. Zerner, ACS, Washington, DC, 1989;
(c) R.G. Parr, W. Yang, Density-functional theory of atoms and molecules, Oxford University Press, Oxford, 1989.
[13] M.J. Frisch, G.W. Trucks, H.B. Schlegel, G.E. Scuseria, M.A. Robb, J.R. Cheeseman, V.G. Zakrzewski, J.A. Montgomery, Jr., R.E. Stratmann, J.C. Burant, S. Dapprich, J.M. Millam, A.D. Daniels, K.N. Kudin, M.C. Strain, O. Farkas, J. Tomasi, V. Barone, M. Cossi, R. Cammi, B. Mennucci, C. Pomelli, C. Adamo, S. Clifford, J. Ochterski, G.A. Petersson, P.Y. Ayala, Q. Cui, K. Morokuma, D.K. Malick, A.D. Rabuck, K. Raghavachari, J.B. Foresman, J. Cioslowski, J.V. Ortiz, A.G. Baboul, B.B. Stefanov, G. Liu, A. Liashenko, P. Piskorz, I. Komaromi, R. Gomperts, R.L. Martin, D.J. Fox, T. Keith, M.A. Al-Laham, C.Y. Peng, A. Nanayakkara, C. Gonzalez, M. Challacombe, P.M.W. Gill, B. Johnson, W. Chen, M.W. Wong, J.L. Andres, C. Gonzalez, M. Head-Gordon, E.S. Replogle, J.A. Pople, Gaussian 98, Revision A.7, Gaussian Inc., Pittsburgh, PA, 1998.
[14] (a) NBO Version 3.1, E.D. Glendening, A.E. Reed, J.E. Carpenter, F. Weinhold;
(b) A.E. Reed, L.A. Curtiss, F. Weinhold, Chem. Rev. 88 (1988) 899.
[15] R.S. Mülliken, J. Chem. Phys. 23 (1955) 1833.
[16] (a) I. Tritto, S.X. Li, M.C. Sacchi, P. Locatelli, G. Zannoni, Macromolecules 28 (1995) 5358;
(b) C.J. Harlan, S.G. Bott, A.R. Barron, J. Am. Chem. Soc. 117 (1995) 6465;
(c) R. Fusco, L. Longo, F. Masi, F. Garbassi, Macromolecules 30 (1997) 7673;
(d) M.L. Ferreira, P.G. Belelli, D.E. Damiani, Macromol. Chem. Phys. 202 (2001) 495.
[17] (a) M.R. Mason, J.M. Smith, S.G. Bott, A.R. Barron, J. Am. Chem. Soc. 115 (1993) 4971;
(b) A. Barron, Macromol. Symp. 97 (1995) 15;
(c) D.E. Babushkin, N.V. Semikolenova, V.N. Panchenko, A.P. Sobolev, V.A. Zakharov, E.P. Talsi, Macromol. Chem. Phys. 198 (1997) 3855;
(d) I.I. Zakharov, V.A. Zakharov, G.M. Zhidomirov, in: W. Kaminsky (Ed.), Metalorganic Catalysts for Synthesis and Polymerization, Springer, Berlin, 1999, p. 129;
(e) H. Sinn, I. Schimmel, M. Ott, N. Von Thienen, A. Harder, W. Hagendorf, B. Heitmann, E. Haupt, in: W. Kaminsky (Ed.), Metalorganic Catalysts for Synthesis and Polymerization, Springer, Berlin, 1999, p. 105.
[18] J. Bliemeister, W. Hagendorf, A. Harder, B. Heitmann, I. Schimmel, E. Shmedt, W. Shnuchel, H. Sinn, L. Tikwe, N. Von Thienen, K. Urlass, H. Winter, O. Zarncke, in: W. Kaminsky (Ed.), Metalorganic Catalysts for Synthesis and Polymerization, Springer, Berlin, 1999, p. 57.
[19] M. Floor, G.M. Smith, D.B. Malpass, Metallocenes Europe 97 (1997) 33.
[20] M. Ystenes, J.L. Eilertsen, J. Liu, M. Ott, E. Rytter, J.A. Støvneng, J. Polym. Sci. Part A: Polym. Chem. 38 (2000) 3106.
[21] (a) B. Rieger, X. Mu, D.T. Mallin, M.D. Rausch, J.C.W. Chien, Macromolecule 23 (1990) 3559;
(b) S. Jüngling, R. Mülhaupt, U. Stehling, H. Brintzinger, D. Fischer, F. Langhauser, J. Polym. Sci. A: Polym. Chem. 33 (1995) 1305;
(c) A. Carvill, I. Tritto, P. Locatelli, M.C. Sacchi, Macromolecule 30 (1997) 7056;
(d) L. D'Agnillo, J.B.P. Soares, A. Penlidis, Macromol. Chem. Phys. 199 (1998) 955;
(e) H.G. Alt, A. Köppl, Chem. Rev. 100 (2000) 1205.
[22] (a) M.L. Ferreira, P.G. Belelli, A. Juan, D.E. Damiani, J. Molec. Catal. A: Chem. 148 (1999) 127;
(b) M.L. Ferreira, P.G. Belelli, A. Juan, D.E. Damiani, Macromol. Chem. Phys. 201 (12) (2000) 1334;
(c) G.M. Zhidomirov, V.B. Kazansky, Advances in Catalysis 34 (1986);
(d) M.M. Branda, N.J. Castellani, Surf. Sci. 393 (1997) 171;
(e) S.P. Yuan, J.G. Wang, Y.W. Li, S.Y. Pen, J. Molec. Catal. A: Chem. 178 (2002) 267.
[23] X. Yang, C.L. Stern, T.J. Marks, J. Am. Chem. Soc. 113 (1991) 3623.
[24] A. Muñoz-Escalona, J. Ramos, V. Cruz, J. Martínes-Salazar, J. Polym. Sci. Part A: Polym. Chem. 38 (2000) 571.
[25] (a) R.F. Jordan, W.E. Dasher, S.F. Echols, J. Am. Chem. Soc. 108 (1986) 1718;
(b) M. Bochmann, S.J. Lancaster, J. Organomet. Chem. 434 (1992) C1;
(c) X. Yang, C.L. Stern, T.J. Marks, J. Am. Chem. Soc. 116 (1994) 1015;
(d) A.K. Rappé, W.M. Skiff, C.J. Casewit, Chem. Rev. 100 (2000) 1435;
(e) L. Resconi, L. Cavallo, A. Fait, F. Piermontesi, Chem. Rev. 100 (2000) 1253;
(f) G.G. Hlatky, Chem. Rev. 100 (2000) 1347;
(g) E.Y.X. Chen, T.J. Marks, Chem. Rev. 100 (2000) 1391.
[26] (a) A.R. Siedle, B. Hangkl, R.A. Newmark, K.R. Mann, T. Wilson, Macromol. Symp. 89 (1995) 299;
(b) W. Kaminsky, Macromol. Chem. Phys. 197 (1996) 3907.
[27] D. Cam, U. Giannini, Makromol. Chem. 193 (1992) 1049.
[28] E. Giannetti, G.M. Nicoletti, R.J. Mazzocchi, J. Polym Sci., Part A: Polym. Chem. 23 (1985) 2117.
[29] (a) K. Prout, T.S. Cameron, R.A. Forder, S.R. Critchley, B. Deuton, G.V. Rees, Acta Crystallogr. B30 (1974) 2290;
(b) L. Resconi, F. Piermontesi, I. Camurati, O. Sudmeijer, I.E. Nifantev, P.V. Ivchenko, L.G. Kuzmina, J. Am. Chem. Soc. 120 (1998) 2308.
[30] K.B. Wiberg, R.F.W. Bader, C.D.H. Lau, J. Am. Chem. Soc. 109 (1987) 985.
[31] (a) S. Niu, M.B. Hall, Chem. Rev. 100 (2000) 360;
(b) M.M. Rohmer, M. Bénard, J.M. Poblet, Chem. Rev. 100 (2000) 509.